ARTICLES
https://doi.org/10.1038/s41565-021-01063-3
nature nanotechnology

Quantitative tracing of uptake and transport of submicrometre plastics in crop plants using lanthanide chelates as a dual-functional tracer

Yongming Luo[1,7] ✉, Lianzhen Li[2,3,7], Yudong Feng[1], Ruijie Li[1,4], Jie Yang[1], Willie J. G. M. Peijnenburg[5,6] and Chen Tu[2,3]

The uptake pathways of nanoplastics by edible plants have recently been qualitatively investigated. There is an urgent need to accurately quantify nanoplastics accumulation in plants. Polystyrene (PS) particles with a diameter of 200 nm were doped with the europium chelate Eu-β-diketonate (PS-Eu), which was used to quantify PS-Eu particles uptake by wheat (*Triticum aestivum*) and lettuce (*Lactuca sativa*), grown hydroponically and in sandy soil using inductively coupled plasma mass spectrometry. PS-Eu particles accumulated mainly in the roots, while transport to the shoots was limited (for example, <3% for 5,000 μg PS particles per litre exposure). Visualization of PS-Eu particles in the roots and shoots was performed with time-gated luminescence through the time-resolved fluorescence of the Eu chelate. The presence of PS-Eu particles in the plant was further confirmed by scanning electron microscopy. Doping with lanthanide chelates provides a versatile strategy for elucidating the interactions between nanoplastics and plants.

According to the diameter of plastic fragments or particles, plastic particles can be classified as microplastics (MPs) and nanoplastics (NPs)[1]. NPs can impose more serious environmental and biological hazards than MPs because their physical dimensions enable them to penetrate biomembrane structures[2–5]. Environmental concentrations of MPs are expected to continue to increase, even if that expectation is based only on the assumption of a steady rate of plastic debris fragmentation[6]. Increasing amounts of small plastic particles directly emitted into the terrestrial environment as well as secondary particles formed by plastic degradation are potential major threats to agricultural (eco)systems.

NPs can interact with plants in many ways, and the accumulation and translocation of NPs as well as their impacts on crop plants and food safety need to be investigated systematically[7]. Although the uptake of PS NPs into plant protoplasts was studied early[8–10], our recent study and other reports have revealed the effective pathways and mechanisms for uptake and translocation of NPs in plants[11–13]. Nevertheless, no quantitative information on uptake kinetics and internal transport of NPs in plants is currently available to the best of our knowledge, despite the fact that this information is a key to assess the environmental impact and the potential hazard of NPs to human health. Previous studies showed various plant responses in terms of growth, chlorophyll contents and/or oxidative stress with NPs exposure[13–17]. This reflects the urgent need to develop new approaches to allow for accurate tracing of NPs and to provide a basis for interpretation of the observed biological responses.

Numerous studies have attempted to track fluorescent particles, such as surface-functionalized PS nanoparticles as a model for NPs[11–13]. However, this technique has a number of disadvantages, including high limits of detection and interference from fluorescent background signals, which is a universal challenge in the visualization of NPs using conventional fluorescence techniques. Furthermore, fluorescence permits qualitative but not accurate quantitative measurement and is greatly affected by numerous external factors, including oxidation, scattering and bleaching[18–20]. Most microscopic imaging techniques allow for only a minute fraction of biological tissues to be qualitatively investigated at the nanometre to micrometre scale. Therefore, an examination of a small fraction of plant tissue by microscopy alone is unlikely to represent the plant as a whole[21]. Radioisotope techniques have recently been successfully used to quantitatively study the fate of plastic nanoparticles at environmentally relevant concentrations[22]. They are, however, of limited applicability because of the hazards involved in dealing with a radioactive substance. Thus, a convenient and cost-effective alternative to radiolabelling that allows for biodistribution to be quantitatively measured could make quantification techniques more accessible to researchers investigating the uptake and translocation of plastic particles by terrestrial organisms.

A promising approach for the identification and quantification of NPs in biological samples by inductively coupled plasma mass spectrometry (ICP-MS) involves doping the plastics with metal elements[23]. Lanthanide chelates are distinctly advantageous, as they have long luminescence lifetimes, large Stokes shifts, sharp emission profiles and visible-light excitation wavelengths[24]. Thus, it is anticipated that such probes could be a useful tool for a broad range of applications in which background-free and time-resolved bioimaging is needed to visualize plastic particles in complex biological samples. Earlier reports have described the utility of lan-

[1]CAS Key Laboratory of Soil Environment and Pollution Remediation, Institute of Soil Science, Chinese Academy of Sciences, Nanjing, China. [2]CAS Key Laboratory of Coastal Environmental Processes and Ecological Remediation, Yantai Institute of Coastal Zone Research, Chinese Academy of Sciences, Yantai, China. [3]Center for Ocean Mega-Science, Chinese Academy of Sciences, Qingdao, China. [4]Northwest Institute of Eco-Environment and Resources, Chinese Academy of Sciences, Lanzhou, China. [5]National Institute of Public Health and the Environment, Center for Safety of Substances and Products, Bilthoven, The Netherlands. [6]Institute of Environmental Sciences (CML), Leiden University, Leiden, The Netherlands. [7]These authors contributed equally: Yongming Luo, Lianzhen Li. ✉e-mail: ymluo@issas.ac.cn

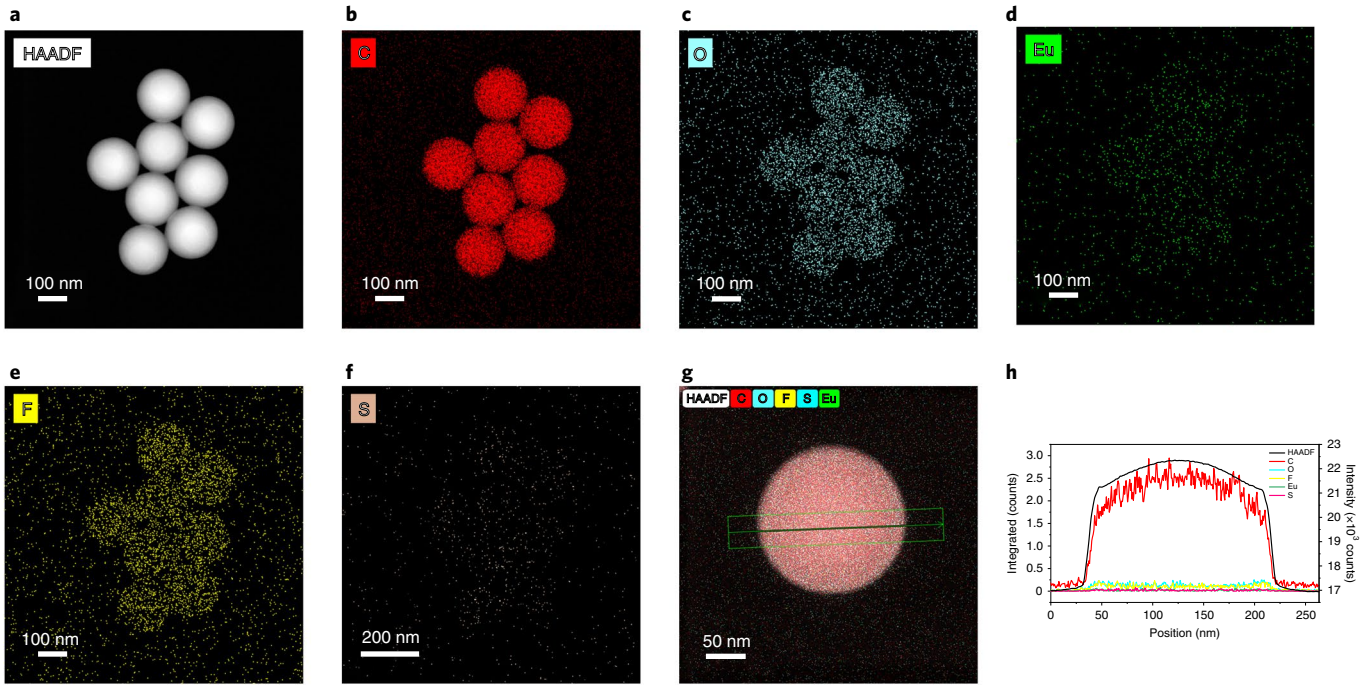

Fig. 1 | PS-Eu particles images and elemental composition. a–f, High-angle annular dark-field (HAADF) STEM image (**a**) and corresponding energy-dispersive X-ray spectroscopy elemental mapping of C (**b**), O (**c**), Eu (**d**), F (**e**) and S (**f**) atoms in the synthesized 0.2 μm PS-Eu particles used in this study. **g**,**h**, Line-scanning profiles (**h**) of C, O, S, F and Eu atoms across the as-prepared PS-Eu particle in the STEM image (**g**).

thanide chelates for the detection of NPs in freshwater mussels and mice using the time-resolved fluorescence from a lanthanide chelate[25,26]. Furthermore, the entrapment of lanthanide chelates within the plastic particles could be a suitable strategy for the indirect determination of the amount of NPs accumulated in the plants via the quantification of lanthanide metals by ICP-MS, even at low concentrations.

This study quantitatively investigated the uptake and translocation of PS particles with a diameter of 200 nm into two crop plants, wheat (*Triticum aestivum*) and lettuce (*Lactuca sativa*). PS is one of the most commonly produced polymers and is used extensively worldwide in the food packaging industry and as a soil conditioner to stabilize soil surface structure and moisture retention[27]. Its detection in organic fertilizers[28], sewage sludges[29] and wastewater[30], which are considered important sources of MPs for terrestrial ecosystems, suggests that it may be broadly present in agricultural soils[31,32]. To simulate different environmental conditions, crop plants were exposed to the PS particles in hydroponic cultures and in sandy soil. A Eu-based, dual-functional probe was applied to the PS particles for the quantification and fluorescence imaging of PS particles. The uptake of PS particles into plants could be accurately and sensitively determined by quantifying the released Eu (which has a very low abundance in the environment) using ICP-MS. Background-free fluorescence imaging was achieved by analysing the characteristic time-resolved fluorescence of the Eu–β-diketonate chelates.

PS-Eu particles characterization

The hydrodynamic diameter of the synthesized PS-Eu and PS particles was determined by dynamic light scattering (DLS) to be 244 ± 12 nm and 260 ± 2 nm, respectively. The PS-Eu and PS particles were spherical, uniform in size and highly monodisperse (Supplementary Fig. 1b,c). The zeta potential of the PS-Eu particles and PS particles was measured to be −14.9 mV and −31.7 mV.

The PS-Eu particles showed strong red photoluminescence upon radiation with ultraviolet (UV) light (Supplementary Fig. 1d, inset). The excitation spectrum was monitored at 612 nm (Supplementary Fig. 1d). At an excitation wavelength of 360 nm, the PS-Eu particles have a typical Eu chelate emission pattern with a primary emission peak at 615 nm (Supplementary Fig. 1e). The lifetime of Eu^{3+} in the PS-Eu particles was estimated as expected to be 841 μs. The decay curve was a single exponential.

Scanning transmission electron microscopy (STEM) with energy-dispersive spectroscopy analysis was used to examine the elemental distribution within the PS-Eu particles. The elemental line scans and maps for C, O, S, F and Eu indicated that tris(thenoyltrifluoroacetonato)europium ($Eu(TTA)_3$) was uniformly distributed throughout the particles (Fig. 1).

Incorporation and stability of Eu chelates in PS particles

Serial dilutions of the PS-Eu particles were prepared for ICP-MS analysis to quantitatively determine Eu concentrations as a function of their mass. Supplementary Fig. 2 shows that the Eu concentration increased linearly with increasing calculated PS-Eu particle mass. The Eu percentage in the particles was estimated to be 1.6 wt% and a load of 2.8×10^5 Eu chelates was obtained per PS-Eu particle. By measuring the Eu concentration of an unknown sample, this relationship could be used to determine the mass (or quantity of particles) of PS-Eu particles. This finding indicates that the directly measured Eu concentration serves as a suitable proxy for the quantity of PS-Eu particles.

The stability of PS-Eu particles was evaluated in a solution by simulating the conditions inside the plant cell environment with the addition of the major ions and some compounds present in the root exudates or inside the plane cells initially adjusted to pH 5.5 or 6.5. No typical Eu chelate emission spectrum was observed in the filtrate of PS-Eu particles suspensions (Supplementary Fig. 3b), indicating that the $Eu(TTA)_3$ encapsulated into the PS particles remain rather stable during exposure. Additionally, there was only a minimal increase in free Eu released during the first two days, but the amount of Eu dissolved did not exceed 0.3 μg l^{-1} for an exposure solution of 5,000 μg l^{-1} PS-Eu particles during a six day period (Supplementary Fig. 3a). This low concentration of Eu^{3+} could not

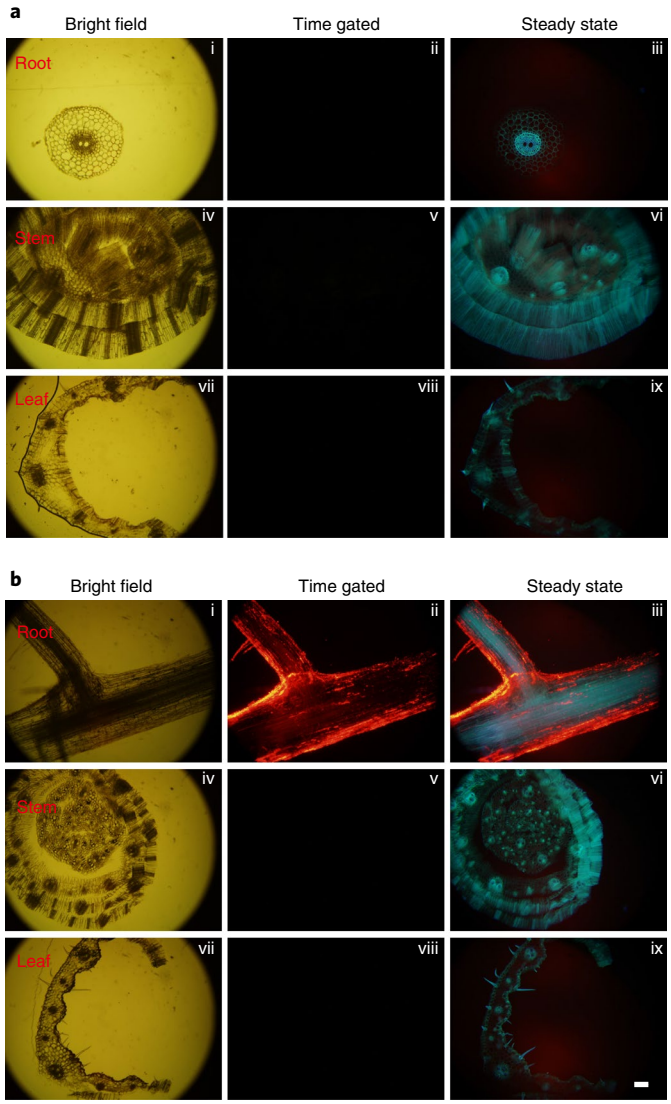

Fig. 2 | Time-gated imaging of wheat root, stem and leaf after exposure to PS-Eu particles. a,**b**, Bright-field images (i, iv, vii), time-gated luminescence images (ii, v, viii) and steady-state luminescence images (iii, vi, ix) of wheat tissues followed by exposure with 50,000 μg l^{-1}, 0.2 μm PS-Eu particles in 20% Hoagland solution for six days (**b**). In a control experiment, wheat plants were exposed to Eu(TTA)$_3$ alone at a Eu concentration approximately equal to 0.3% leakage (referring to Supplementary Fig. 3a, determined in a separate Eu leaching experiment) from the exposure concentration of PS-Eu particles in solution that was used (**a**). Scale bar, 100 μm.

lead to any significant Eu accumulation in wheat and lettuce plants relative to the control plants ($P < 0.05$; Fig. 4a,b, inset). The very minimal Eu leaching from the particles indicated that Eu was sufficiently bound (or incorporated) in Eu(TTA)$_3$, which was used as a conservative tracer, within the polymer.

Theoretical calculations could permit reasonably good estimates of relative binding strengths and stability of the metal complex. It has been observed that calculated energy differences can correctly predict the relative stability constant by linear correlation[33]. From simplified density functional theory calculations[34], it can be qualitatively predicted that the chelating strength of TTA towards Eu^{3+} is much stronger than that towards a hydrogen ion, as well as that towards the alkali and alkaline earth metal cations present in the plant or exposure medium (Supplementary Table 1), and it is energetically favourable for Eu^{3+} to be chelated by multiple TTA, which is consistent with previous reported trends[35]. This further suggests that the Eu complexes encapsulated into the PS particles are relatively stable in the exposure environment.

Fluorescence imaging of PS-Eu particles in plants

Wheat and lettuce seedlings treated with different concentrations (ranging from 0 to 50,000 μg l^{-1}) of PS-Eu particles were measured under 365 nm UV light excitation. In contrast to the control group, wherein no fluorescence was exhibited, red fluorescence was observed in the plant roots exposed to PS-Eu particles (Supplementary Fig. 4a,c). Plant roots emitted clear dose-dependent red fluorescence throughout the entire root under 365 nm UV light (Supplementary Fig. 4a,c), thus providing direct evidence of increased absorption of PS-Eu particles by lettuce and wheat as the concentration increased. Red fluorescence in the leaves was not observed until the PS-Eu particles concentration reached 50,000 μg l^{-1} (Supplementary Fig. 4b,d). Unlike wheat, wherein PS-Eu particles was located in the leaf vasculature (Supplementary Fig. 4b), PS-Eu particles was found mainly in the leaf margin of lettuce (Supplementary Fig. 4d), suggesting that PS-Eu particles pass easily through the lettuce leaf veins to the end of the vascular bundle with water flow and accumulates in the cells at this point of exit.

The time-gated luminescence technique, which makes use of long-lived luminescent probes (for example, lanthanide complexes) and time-delayed detection, substantially enhances the signal-to-noise ratio and contrast by suppressing the autofluorescence contribution[36]. In the absence of time-gated luminescence detection, as shown in Figs. 2b(iii) and 3b(iii), the root tissues emitted strong blue autofluorescence under UV excitation. The red luminescence of the probes overlapped with the blue autofluorescence of the plant tissues, which made it difficult to unambiguously identify the locations of the PS-Eu particles. By applying time-gated detection, as shown in Figs. 2b(ii) and 3b(ii) the background autofluorescence was substantially suppressed, allowing for highly specific and background-free images of the plants exhibiting strong red luminescence to be recorded. No strong fluorescence was observed in the stems or leaves of the plants (as shown in Figs. 2b(v),(viii), respectively, and 3b(v),(viii), respectively). A control experiment was included with Eu(TTA)$_3$ exposure alone at a concentration at which the Eu content was approximately equal to that released from the exposure concentration of PS-Eu particles in solution that was used (Figs. 2a and 3a), which showed no typical Eu chelate fluorescence.

Strong red luminescence signals are emitted from the root epidermis. This result indicates that the PS-Eu particles were transported to and located in this organ of the plants. Moreover, a number of red areas were observed in the cortex and vascular tissues of the lettuce plants exposed to PS-Eu particles (Fig. 3b(ii)). Similar results were obtained for the wheat plants (Fig. 2b(ii)). Only very low fluorescence signals were detected in the stems and leaves of the plants (Fig. 3b(v),(viii)). A strong red luminescence signal was detected in the cracks present in the wheat lateral root zone (Fig. 2b(ii)) where the lateral roots penetrate the endodermis and the cortex. This indicated that these cracks were the major entry sites into the root for the PS-Eu particles[11].

Uptake into plants and biodistribution of PS-Eu particles in plants

Eu was detected in the lettuce and wheat plants at a concentration as low as 5 μg l^{-1} PS particles in solution. This concentration was previously predicted as a possible environmental concentration of NPs[37]. Exposure of Eu(TTA)$_3$ or Eu^{3+} alone at a Eu concentration approximately equal to 0.3% leakage (referring to Supplementary Fig. 3a, determined in a separate Eu leaching experiment) from the 5,000 μg l^{-1} PS-Eu particles exposure concentration that was used could not lead to significant Eu accumulation in wheat and lettuce

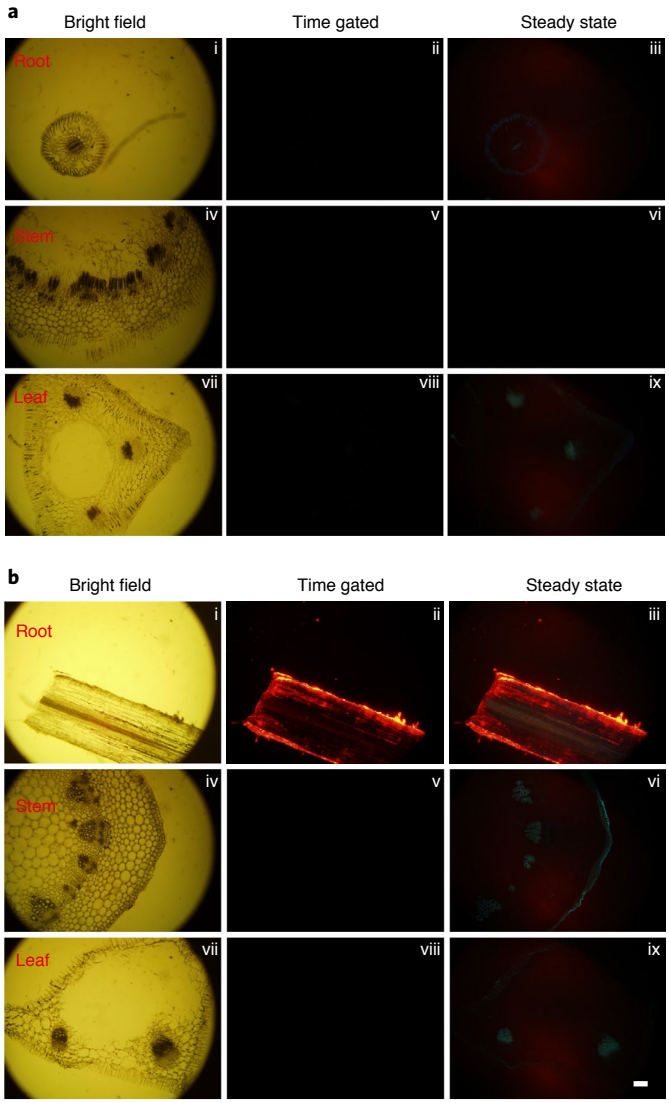

Fig. 3 | Time-gated imaging of lettuce root, stem and leaf after exposure to PS-Eu particles. a,**b**, Bright-field images (i, iv, vii), time-gated luminescence images (ii, v, viii) and steady-state luminescence images (iii, vi, ix) of lettuce tissues followed by exposure with 50,000 μg l^{-1}, 0.2 μm PS-Eu particles in 20% Hoagland solution for six days (**b**). In a control experiment, lettuce plants were exposed to Eu(TTA)$_3$ alone at a Eu concentration approximately equal to 0.3% leakage (referring to Supplementary Fig. 3a, determined in a separate Eu leaching experiment) from the exposure concentration of PS-Eu particles in solution that was used (**a**). Scale bar, 100 μm.

plants relative to the control ($P < 0.05$; Fig. 4a,b, inset). The majority of the PS-Eu particles accumulated in the roots (~1.3–1,494 μg g^{-1} dry weight for wheat and ~4.1–2,220 μg g^{-1} dry weight for lettuce; Fig. 4a,b). Supplementary Table 2 shows the amount of Eu present in each phase (that is, exposure media, adsorption to exposure vessel, adsorption to roots, absorption on the roots and translocation to shoot tissues) after six days of exposure to 5,000 μg l^{-1} PS-Eu particles, as well as the total Eu amount that enters the experimental system during this period. For both wheat and lettuce plants, more than 89% of the amount of Eu entering the system was recovered in the amount of Eu leaving the system. This showed that only a limited amount of PS-Eu particles could be translocated to the shoots (<3%), although a substantial amount was associated with the roots (Supplementary Table 2).

There was no detectable leakage of Eu in the soil leachates or soil solution, suggesting that PS-Eu particle was stable in soils. The plants showed notable uptake of PS-Eu particles in the roots with an average bioconcentration factor of 1.8 for wheat and 2.9 for lettuce after 14 days exposure in 1 mg kg^{-1} and 10 mg kg^{-1} PS-Eu particles in a sandy soil (Fig. 4c). The root PS-Eu particles concentration was ~3.0–5.2 μg g^{-1} dry weight in wheat and ~4.3–15.2 μg g^{-1} dry weight in lettuce. Although the root concentration of PS-Eu particles in the soil culture was much lower than those observed in the hydroponic culture, they showed notable translocation to the shoots, with average translocation factors of 0.09 and 0.14 for wheat and lettuce, respectively.

Biological effects after exposure

A direct comparison between exposure of PS-Eu and PS particles (similar in size and surface charge) showed no obvious effects on the plant growth (Supplementary Fig. 5) or on net photosynthesis rate, stomatal conductance or transpiration rate within the tested concentrations less than 5,000 μg l^{-1} in the hydroponic solution ($P < 0.05$; Supplementary Tables 3 and 4). The catalase activities in root tissues of wheat and lettuce were slightly higher than those recorded for control seedlings (Supplementary Fig. 6). A slight increase in total organic carbon was found in the nutrient solution of plants exposed to PS-Eu particles compared to the controls (Supplementary Tables 5 and 6), indicating that the plants exudate low-molecular-weight chemicals in response to exposure of PS-Eu particles.

Observation of PS-Eu particles in plants by microscopy

The uptake of PS-Eu particles by the wheat and lettuce plants was also supported by scanning electron microscopy (SEM) observations of the roots and shoots of the plants after exposure to 50,000 μg l^{-1} PS-Eu particles. The SEM images clearly confirmed that aggregation of the 0.2 μm PS-Eu particles was mostly confined to the xylem and cell walls of the cortex tissue of the wheat (Fig. 5a–f) and lettuce (Fig. 6) roots, though some particles were observed in the wheat leaves as well (Fig. 5g–i). These observations indicate that once the PS particles entered the vascular cylinder of the roots, they could readily move along the vascular bundle with the water and nutrient flow and be further transported to the stems and leaves.

Discussion

NPs pollution is a novel issue for the agricultural fields, and uptake of NPs by crop species has recently received an increasingly high degree of scientific and social concern[7]. Characterizing the processes occurring in crop plants exposed to NPs is urgently needed to model the environmental impact and biological fate of NPs in agricultural ecosystems. A quantitative understanding of these processes represents a basis for further hazard and risk assessment of NPs under realistic environmental conditions. Nevertheless, the accurate quantification and visualization of NPs in complex plant system remain a substantial challenge that has not been fully addressed at this point.

The proposed approach of labelling NPs with lanthanide chelates represents a simple and effective way to trace the uptake and translocation of plastic particles in complex biological media. The Eu element doping allows the indirect quantification of NPs in plant tissue, which is a highly important, currently unsolved problem in the field of NPs research. Moreover, this is a highly promising approach as no complicated synthesis is needed. Furthermore, due to the time-dependent luminescence of Eu chelates, the Eu chelates doping also allows background-free fluorescence imaging. This is crucial to circumvent problems with the strong autofluorescence of plant tissues. PS-Eu particles made with Eu(TTA)$_3$ was chosen as a luminophore because of its high luminescence quantum yield, stability and solubility in aqueous buffers[38]. To the best of our knowledge, we

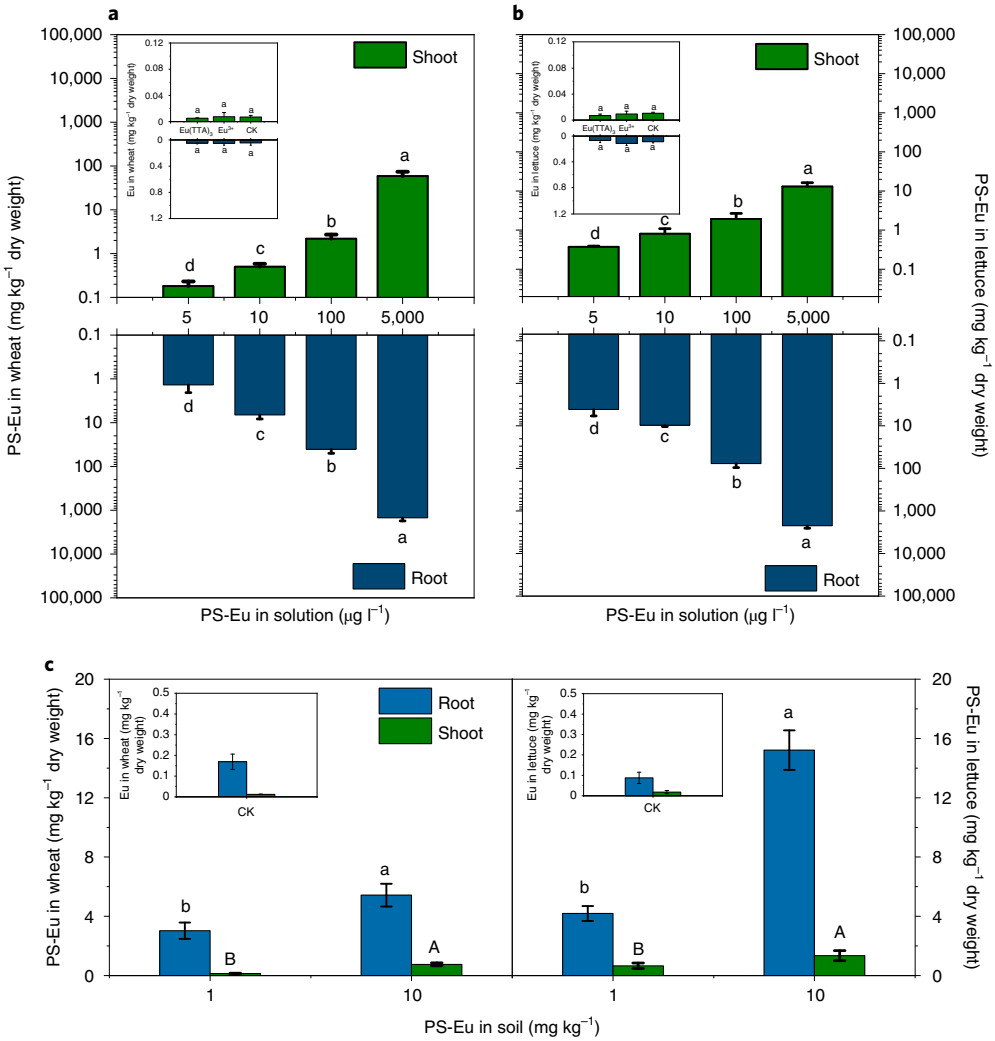

Fig. 4 | Bioaccumulation of PS-Eu particles in two crop plants after exposure in solution and soil. a,**b**, Bioaccumulation of 0.2 μm PS-Eu particles in roots and shoots of wheat (**a**) and lettuce (**b**) grown for six days with different concentrations of PS-Eu particles in solution. **c**, Bioaccumulation of 0.2 μm PS-Eu particles in roots and shoots of wheat (left) and lettuce (right) grown for 14 days with 1 mg kg^{-1} and 10 mg kg^{-1} PS-Eu particles in a sandy soil. Lettuce and wheat seedlings were grown in 20% Hoagland solutions, with PS-Eu particles with concentrations of 5, 10, 100 and 5,000 μg l^{-1}. Control experiments (insets) were done in solution including exposure to Eu(TTA)$_3$ or Eu^{3+} alone at a Eu concentration approximately equal to 0.3% leakage (Supplementary Fig. 3a, determined in a separate Eu leaching experiment) from the 5,000 μg l^{-1} PS-Eu particles exposure concentration used in solution. Hoagland solution exposure was used as CK. Plants grown in soil that did not contain the PS-Eu particles were used as CK in soil exposure. The concentration of Eu determined by ICP-MS was converted to the concentration of PS-Eu particles using the linear equation (Supplementary Fig. 2) obtained using exogenous PS-Eu particles after subtracting the background Eu value from the control (insets). Data are given as mean ± s.d. (n = 3). Different letters represent statistically significant differences among treatments (P < 0.05), as revealed using one-way analysis of variance followed by the Duncan's post-hoc test. In soil exposure, different lowercase letters and uppercase letters indicate significant among the means of the PS-Eu particle content in the root and shoot (P < 0.05).

present here a new lanthanide-metal-based labelling technique that is used to quantify and visualize the uptake of submicrometre-sized plastics in two crop plants (lettuce and wheat). This may facilitate future quantitative studies on NPs–plant interactions.

The labelling approach described here, on the basis of highly sensitive ICP-MS, may provide a valuable technique by which to investigate the biological fate of NPs in plants at low environmental concentrations. Our results showed that even at a concentration of 5 μg l^{-1}, PS-Eu particles accumulated in the plant's root and transported to the shoot could subsequently be detected using ICP-MS. There is currently no information on the environmental concentrations of NPs to the best of our knowledge, since the currently available analytical methods do not yet permit for accurate detection of nano-sized and even submicrometre-sized plastic particles in the environment. Thus, it remains challenging to conclude that the experimental exposures in this study are likely to mimic environmental conditions in terms of NPs contamination. However, we were able to decrease from the commonly used exposure concentrations of up to 10 mg l^{-1} (refs. [11,15]), used in studies attempting to detect NPs in plants, by a factor of 2,000.

The absence of significant impacts on plant growth found in the two plants is in accordance with previous studies, showing no significant effects for growth of *Allium cepa*[14] and *Vicia faba*[16] exposed to doses up to 100 mg l^{-1}. The slight alterations in antioxidant levels may be a protection mechanism against reactive oxygen species (ROS) production associated with oxidative stress after exposure[13]. A direct comparison between exposure of PS-Eu and unlabelled PS particles (similar in size and surface charge) showed that the small amount of Eu doped in the PS particle has no significant impact on plant growth or on photosynthesis parameters and antioxidant activity. PS-Eu

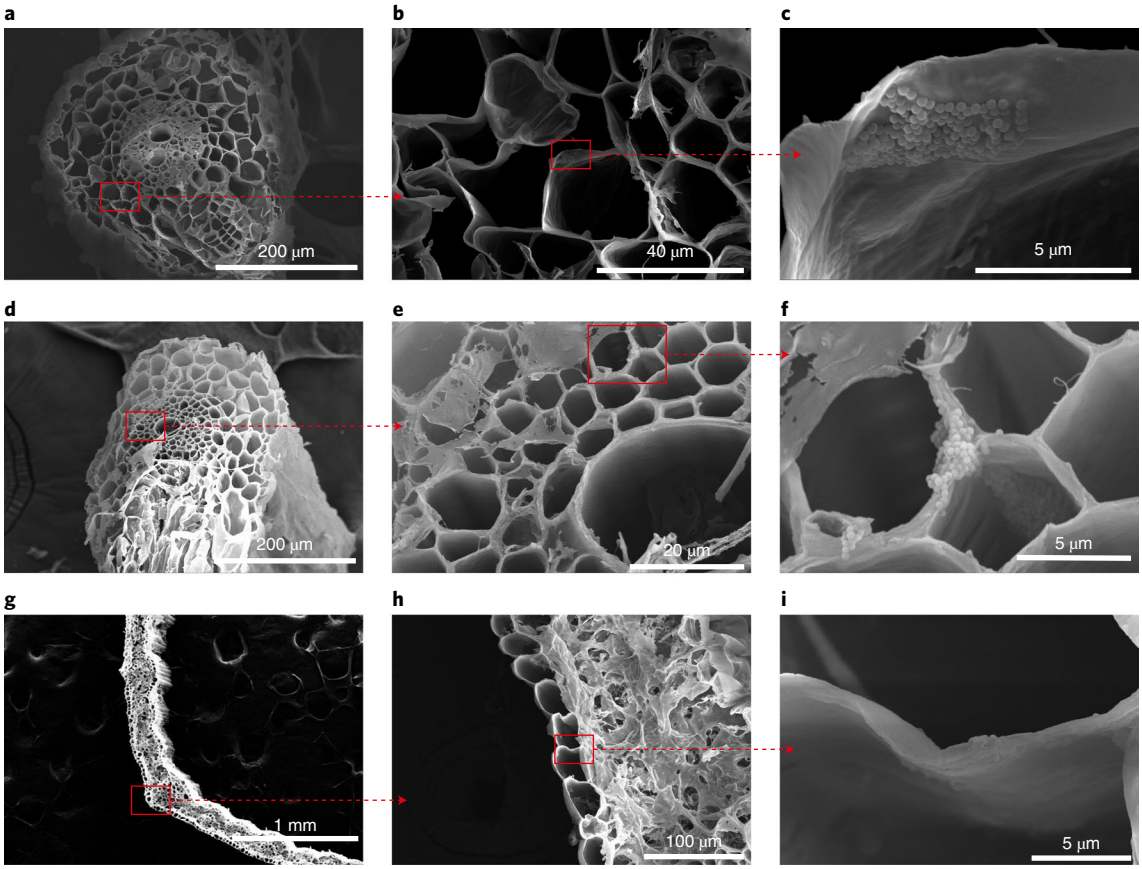

Fig. 5 | SEM images of PS-Eu particles localization in the root and leaf of a wheat plant. a–f, Localization in the root. **g–i**, Localization in the leaf. Two-week-old wheat plants were exposed to 50,000 µg l^{-1}, 0.2 µm PS-Eu particles for six days. Each arrow indicates a magnified view of the area inside the red square.

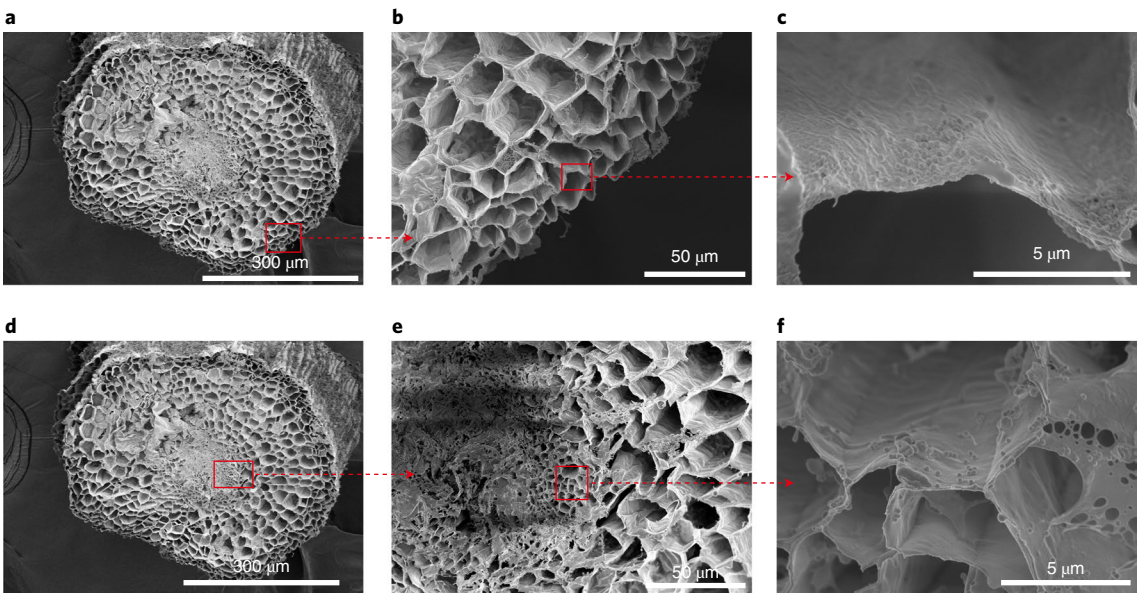

Fig. 6 | SEM images of PS-Eu particles localization in the root of a lettuce plant. a–f, SEM images at various magnifications. One-month-old lettuce plants were exposed to 50,000 µg l^{-1}, 0.2 µm PS-Eu particles for six days. Each arrow indicates a magnified view of the area inside the red square.

particles were agglomerated during plant exposure (Supplementary Table 7 and Supplementary Fig. 7), due to the combined effects of cations and root exudates. The root cap can secrete large amounts of mucilage (a highly hydrated polysaccharide) to defend the plant against pathogens[39]. A report showed that exposure to PS NPs increases the exudation of oxalate in *Arabidopsis thaliana*[13].

The two crop plants demonstrated the ability to substantially bioaccumulate the PS-Eu particles on the roots. However, only a

limited amount of PS-Eu particles was translocated to the edible parts. There was less uptake of PS-Eu particles on the roots in wheat than in lettuce. The difference in uptake and transfer to shoots among different (crop) plant species should be investigated in the future, as it is plausible that physiological variation among plant species, such as differences in root exudates, transpiration rate, hydraulic conductivity and the structure, composition and pore size of the cell wall[40], might influence the transport and accumulation of plastic particles.

Although rare-earth-metal labelling strategies have been previously proposed for the detection of NPs in environmental media[23], their application in plants has not yet been considered, to the best of our knowledge. This method, which combines fluorescence imaging and ICP-MS-based quantitative bioanalysis, integrates the advantages of these two common analytical techniques. The particles synthesized in this study cannot ultimately act as direct analytical tools to determine NPs uptake and translocation in a realistic environment. Nevertheless, by providing the opportunity to quantitatively track and measure trace concentrations of plastic particles in biological systems, this approach can promote our understanding of the biological uptake and translocation of NPs at concentrations as low as those that have been predicted previously as possible environmental concentrations of NPs[37]. The accurate quantification and microscopic visualization of different NPs using this method elucidates their unique effects on biota, such as the effects dependent on their shape, size and surface (coating or corona).

Conclusions

We successfully developed a lanthanide labelling technique and used it to quantify the uptake of submicrometre plastics in two crop plants (lettuce and wheat). PS-Eu particles were easily synthesized and accurately quantified and visualized within the crop plants due to the excellent ICP-MS response of lanthanide metals and the unique luminescence of the lanthanide chelate. Using the labelling method, this study showed that a transfer of NPs (and uptake) into the plants occurs, but no notable biomagnification was observed. The method can be extended to other types of NPs found in the environment, which may facilitate future quantitative studies on NPs–plant interactions and will benefit ongoing quantitative environmental risk assessments of NPs. The labelling technology used in this study could also be applied in microcosm or mesocosm experiments to enhance the sensitivity of NPs detection. However, potential lanthanide leaching from the particles should be monitored carefully in the systems due to the complex environmental conditions as well as due to the presence of a wide number of (micro)organisms.

Online content

Any methods, additional references, Nature Research reporting summaries, source data, extended data, supplementary information, acknowledgements, peer review information; details of author contributions and competing interests; and statements of data and code availability are available at https://doi.org/10.1038/s41565-021-01063-3.

Received: 25 May 2021; Accepted: 26 November 2021;
Published online: 20 January 2022

References

1. Wallace, H. Presence of microplastics and nanoplastics in food, with particular focus on seafood. *EFSA J.* **14**, e04501 (2016).
2. Fahn, A. *Plant Anatomy* (Pergamon, 1982).
3. Jeong, C. B. J. et al. Microplastic size-dependent toxicity, oxidative stress induction, and p-JNK and p-p38 activation in the monogonont rotifer (*Brachionus koreanus*). *Environ. Sci. Technol.* **50**, 8849–8857 (2016).
4. Le, L. L. et al. Polystyrene (nano)microplastics cause size-dependent neurotoxicity, oxidative damage and other adverse effects in *Caenorhabditis elegans*. *Environ. Sci. Nano.* **5**, 2009–2020 (2018).
5. Mateos-Cardenas, A., van Pelt, F. N. A. M., O'Halloran, J. & Jansen, M. A. K. Adsorption, uptake and toxicity of micro- and nanoplastics: effects on terrestrial plants and aquatic macrophytes. *Environ. Pollut.* **284**, 117183 (2021).
6. de Souza Machado, A. A., Kloas, W., Zarf, C., Hempel, S. & Rillig, M. C. Microplastics as an emerging threat to terrestrial ecosystems. *Glob. Chang. Biol.* **24**, 1405–1416 (2018).
7. Rillig, M. C., Lehmann, A., de Souza Machado, A. A. & Yang, G. Microplastic effects on plants. *New Phytol.* **223**, 1066–1070 (2019).
8. Mayo, M. A. & Cocking, E. C. Pinocytic uptake of polystyrene latex particles by isolated tomato fruit protoplasts. *Protoplasma* **68**, 223–230 (1969).
9. Eicherta, T., Kurtza, B. A., Steinerb, U. & Goldbach, H. E. Size exclusion limits and lateral heterogeneity of the stomatal foliar uptake pathway for aqueous solutes and water suspended nanoparticles. *Physiol. Plant.* **134**, 151–160 (2008).
10. Etxeberria, E., Gonzalez, P., Baroja-Fernández, E. & Romero, J. P. Fluid phase endocytic uptake of artificial nano-spheres and fluorescent quantum dots by sycamore cultured cells. *Plant Signal. Behav.* **1**, 196–200 (2006).
11. Li, L. Z. et al. Effective uptake of submicrometre plastics by crop plants via a crack-entry mode. *Nat. Sustain.* **3**, 929–937 (2020).
12. Sun, H. F., Lei, C. L., Xu, J. H. & Li, R. L. Foliar uptake and leaf-to-root translocation of nanoplastics with different coating charge in maize plants. *J. Hazard. Mater.* **416**, 125854 (2021).
13. Sun, X. D. et al. Differentially charged nanoplastics demonstrate distinct accumulation in *Arabidopsis thaliana*. *Nat. Nanotechnol.* **15**, 755–760 (2020).
14. Jiang, X. F. et al. Ecotoxicity and genotoxicity of polystyrene microplastics on higher plant *Vicia faba*. *Environ. Pollut.* **250**, 831–838 (2019).
15. Lian, J. P. et al. Impact of polystyrene nanoplastics (PSNPs) on seed germination and seedling growth of wheat (*Triticum aestivum* L.). *J. Hazard. Mater.* **385**, 121620 (2020).
16. Giorgetti, L. et al. Exploring the interaction between polystyrene nanoplastics and *Allium cepa* during germination: internalization in root cells, induction of toxicity and oxidative stress. *Plant Physiol. Biochem.* **149**, 170–177 (2020).
17. Bosker, T., Bouwman, L. J., Brun, N. R., Behrens, P. & Vijver, M. G. Microplastics accumulate on pores in seed capsule and delay germination and root growth of the terrestrial vascular plant *Lepidium sativum*. *Chemosphere* **226**, 774–781 (2019).
18. Liu, Y., Ma, W. H. & Wang, J. Theranostics of gold nanoparticles with an emphasis on photoacoustic imaging and photothermal therapy. *Curr. Pharm. Des.* **24**, 2719–2728 (2018).
19. Leblond, F., Davis, S. C., Valdes, P. A. & Pogue, B. W. Pre-clinical whole-body fluorescence imaging: review of instruments, methods and applications. *J. Photochem. Photobiol. B* **98**, 77–94 (2010).
20. Zheng, Q. & Lavis, L. D. Development of photostable fluorophores for molecular Imaging. *Curr. Opin. Chem. Biol.* **39**, 32–38 (2017).
21. González-Melendi, P. et al. Nanoparticles as smart treatment-delivery systems in plants: assessment of different techniques of microscopy for their visualization in plant tissues. *Ann. Bot.* **101**, 187–195 (2008).
22. Al-Sid-Cheikh, M. et al. Uptake, whole-body distribution, and depuration of nanoplastics by the scallop *Pecten maximus* at environmentally realistic concentrations. *Environ. Sci. Technol.* **52**, 14480–14486 (2018).
23. Mitrano, D. M. et al. Synthesis of metal-doped nanoplastics and their utility to investigate fate and behaviour in complex environmental systems. *Nat. Nanotechnol.* **14**, 362–368 (2019).
24. Weissman, S. I. Intramolecular energy transfer the fluorescence of complexes of europium. *J. Chem. Phys.* **10**, 214–215 (1942).
25. Crawford, L., Higgins, J. & Putnam, D. A simple and sensitive method to quantify biodegradable nanoparticle biodistribution using europium chelate. *Sci. Rep.* **5**, 13177 (2015).
26. Facchetti, S. V. et al. Detection of metal-doped fluorescent PVC microplastics in freshwater mussels. *Nanomaterials* **10**, 2363 (2020).
27. Maghchiche, A., Haouam, A. & Immirzi, B. Use of polymers and biopolymers for water retaining and soil stabilization in arid and semiarid regions. *J. Taibah. Univ. Sci.* **4**, 9–16 (2010).
28. Weithmann, N. et al. Organic fertilizer as a vehicle for the entry of microplastic into the environment. *Sci. Adv.* **04**, eaap8060 (2018).
29. Yang, J. et al. Microplastics in an agricultural soil following repeated application of three types of sewage sludge: a field study. *Environ. Pollut.* **289**, 117943 (2021).
30. Murphy, F., Ewins, C., Carbonnier, F. & Quinn, B. Wastewater treatment works (WwTW) as a source of microplastics in the aquatic environment. *Environ. Sci. Technol.* **50**, 5800–5808 (2016).
31. Chen, Y. L., Leng, Y. F., Liu, X. N. & Wang, J. Microplastic pollution in vegetable farmlands of suburb Wuhan, central China. *Environ. Pollut.* **257**, 113449 (2019).
32. Helcoski, R., Yonkos, L. T., Sanchez, A. & Baldwin, A. H. Wetland soil microplastics are negatively related to vegetation cover and stem density. *Environ. Pollut.* **256**, 113391 (2020).
33. Vukovic, S., Hay, B. P. & Bryantsev, V. S. Predicting stability constants for uranyl complexes using density functional theory. *Inorg. Chem.* **54**, 3995–4001 (2015).

34. Adamo, C. & Barone, V. Toward reliable density functional methods without adjustable parameters: the PBE0 model. *J. Chem. Phys.* **110**, 6158–6169 (1999).
35. Smith, R. M. & Martell, A. E. *Critical Stability Constants* Vol. 3 Other Organic Ligands 249 (Plenum, 1977).
36. Song, B. et al. Background-free *in-vivo* imaging of vitamin C using time-gateable responsive probe. *Sci. Rep.* **5**, 14194 (2015).
37. Lenz, R., Enders, K. & Nielsen, T. G. Microplastic exposure studies should be environmentally realistic. *Proc. Natl Acad. Sci. USA* **113**, E4121–E4122 (2016).
38. Latva, M. et al. Correlation between the lowest triplet state energy level of the ligand and lanthanide (III) luminescence quantum yield. *J. Lumin.* **75**, 149–169 (1997).
39. Wen, F. S., VanEtten, H. D., Tsaprailis, G. & Hawes, M. C. Extracellular proteins in pea root tip and border cell exudates. *Plant Physiol.* **143**, 773–783 (2007).
40. Burton, R. A., Gidley, M. J. & Fincher, G. B. Heterogeneity in the chemistry, structure and function of plant cell walls. *Nat. Chem. Biol.* **6**, 724–732 (2010).

Methods

$Eu(TTA)_3$ incorporation into PS particles. The europium complex, $Eu(TTA)_3$, was custom synthesized from Shanghai Huge Biotechnology Company for incorporation into the PS particles according to a previously reported procedure[41]. Briefly, 2 mM $EuCl_3$ (20 ml, Aladdin Reagent) was added to 30 ml of ethanol containing thenoyltrifluoroacetone (6 mM; pH adjusted to 7.0 with 2 M NaOH). The solution was heated to 60 °C under magnetic stirring. A precipitate was immediately observed, and agitation was continued for 1 h at 60 °C. Finally, the Eu complex was obtained by filtration, washed with deionized water and dried in an oven at 70 °C overnight. PS particles (0.2 μm) were custom synthesized via an emulsion polymerization process[42] from Shanghai Huge Biotechnology Company. PS-Eu particles were prepared via a combined swelling–diffusion technique. This technique involves trapping $Eu(TTA)_3$ on a microparticle surface by introducing an organic solvent that swells the microparticle, followed by deswelling (Supplementary Fig. 1a). $Eu(TTA)_3$ was first dissolved in methanol (30 ml). A second suspension containing the 0.2 μm pristine PS particles (100 ml) was added to acetone as a swelling agent, and the solution was adjusted to a pH of 7.0 with NaOH (2 M). The first solution was heated to 90 °C under magnetic stirring, and was then added to the second solution. After stirring for 40 min, the solution was allowed to cool slowly to room temperature. The solutions were then filtered using a glass fibre filter to produce luminescent PS particles (PS-Eu). The particles were treated with dialysis to remove any free Eu that was not incorporated into the polymer particles using membrane tubing (Spectrum Labs) with a molecular weight cut-off of 3,000 Da.

Characterization of PS-Eu particles. The shape and morphology of the obtained PS-Eu particles were investigated by high-angle annular dark-field STEM with energy-dispersive spectroscopy mapping (Thermo Fisher Scientific, Talos F200XG2). The elemental composition of the particles was confirmed by the energy-dispersive spectroscopy mapping analysis. The average hydrodynamic diameter and zeta potential of the PS-Eu particles dispersed in Hoagland solution[43] were determined by DLS using a Malvern Zetasizer Nano-ZS90 (ZEN3590).

To determine the concentration of Eu in the PS-Eu particles, PS-Eu particles stock solutions (10 mg ml^{-1}) were diluted with ultrapure deionized H_2O in glass vials with tightly fitting lids, considering different dilution factors. The particles were then digested for analysis with a mixture of HNO_3 and H_2SO_4 (8:1 v/v, 4.5 ml) and heated to 180 °C for 6 h until a clear solution was obtained. Then, the solution was diluted with ultrapure deionized H_2O for ICP-MS analysis (Agilent 7500i, Agilent Technologies).

Excitation and emission photoluminescence spectra were recorded with a FluoroMax-4 Spectrofluorometer (Horiba Scientific). Time-gated luminescence measurements were carried out on a Perkin-Elmer Victor 1420 multilabel counter with an excitation wavelength of 360 nm, emission wavelength of 615 nm, delay time of 0.2 ms, window time (counting time) of 0.4 ms and cycling time of 1.0 ms.

PS-Eu particle stability. The stability of the PS-Eu particles was determined in a solution that simulated the conditions inside the plant cell environment by exposing the PS-Eu particles (5,000 μg l^{-1}) to a nutrient solution containing 2.5 mM $Ca(NO_3)_2$, 1 mM $MgSO_4$, 2.5 mM KNO_3, 0.1 mM K_2HPO_4, 5 mM NaCl, 50 μM glucose, 25 μM oxalic acid, 12.5 μM serine and 5.0 μM sodium iron chlorophyllin for six days. The PS-Eu particles were dispersed in solutions initially adjusted to pH 5.5 or 6.5. We then monitored Eu leaching from the PS particles in the exposure medium using a centrifugal ultrafiltration technique at zero, one, two, four and six days. The centrifugal filter units (Amiconultra, 3 kDa molar mass cut-off) were first pre-equilibrated with the experimental medium used for plant exposures. Subsequently, 4 ml of each sample was centrifuged at 3,700*g* for 20 min. To ensure that adsorptive losses of Eu were negligible, both the supernatant and the filtrate were discarded and the protocol was repeated three times. Following the fourth centrifugation cycle, potential leaked Eu was determined in the filtrate. The potential Eu chelate release from the particles in the exposure medium was also analysed through a syringe filter unit (Millex, 0.1 μm). The emission spectra was analysed in the filtrate using a FluoroMax-4 Spectrofluorometer (Horiba Scientific) equipped with a 1 cm quartz cell at 25 °C, with excitation and emission slit widths of 5 nm each and the excitation wavelength at 360 nm.

Theoretical calculations permit reasonably good estimates of relative binding strengths and stability of metal complexes. Density functional theory calculations were carried out with the PBE0 functional with the Stuttgart/Dresden pseudopotential and basis set for metal and 6-31G* basis set for the rest atoms using Gaussian 16 (refs. [44–46]). A thermodynamic cycle approach was adopted for the complexation free energy calculation (ΔG_{aq}). These values were then used to calculate aqueous relative stability constants ($\log(\beta)$) according to equation (1), where a_M, a_L and a_{ML} are the activities of the metal ion, ligand and metal complex, R is the gas constant and T is the absolute temperature.

$$\log\beta = \log\frac{[ML]}{[M]\,[L]} \approx \log\frac{a_{ML}}{a_M a_L} = \frac{-\Delta G_{aq}}{2.303RT} \quad (1)$$

Plant culture and PS-Eu particles exposure. Wheat (*T. aestivum* L.) and lettuce (*L. sativa* L.) seeds were used in this study. Wheat seeds of nearly uniform size were surface sterilized by treatment with a 10% NaClO solution for 5 min. Subsequently, the seeds were washed three times with deionized water to remove residual NaClO solution, transferred to moistened filter paper and incubated in the dark at 25 °C to induce germination. After four days, four seedlings of uniform size were transferred to a 1 l beaker containing 1/5 strength Hoagland solution adjusted to pH 6.5, controlled using 2 mmol l^{-1} 2-(*N*-morpholino) ethane sulfonic acid buffering. The beaker was covered with a cap and placed in a growth chamber at 25 ± 2 °C with illumination (250 μmol m^{-2} s^{-1}), a 12-h-day/12-h-night photoperiod and 80% relative humidity. After seven days, the wheat plants were placed in 100 ml beakers (three seedlings in each group) and exposed to different PS-Eu particle concentrations (0, 5, 10, 100 and 5,000 μg l^{-1}) for six days. The experiment was repeated three times.

Lettuce seeds were surface sterilized with a 10% NaClO solution for 5 min and washed three times with deionized water. Subsequently, the seeds were germinated and grown in organic soil (potting mix) in a greenhouse (65% relative humidity) at 25 ± 2 °C with a 16-h-day/8-h-night photoperiod for 21 days. The plants were removed from the soil, and the roots were carefully washed with water until no soil was visible on their surfaces. The exposure methods were the same as those for the wheat seedlings except for the following: Two plants were allocated to a 1 l beaker containing Hoagland solution and allowed to grow for one week before treatment with the PS-Eu particles. After one week, the initial Hoagland solution was replaced with Hoagland solution containing the same PS-Eu particle concentrations as those used for wheat exposure. Plants grown in Hoagland solution that did not contain the PS-Eu particles were used as controls. The plants were grown for six days before being evaluated. Each treatment was replicated three times. In parallel, plant seedlings were exposed to Eu^{3+} alone (supplied as $Eu(NO_3)_3$) in solution, and the plants were sampled at six days to determine the Eu content. The Eu^{3+} concentrations was approximately equal to 0.3% leakage (Supplementary Fig. 3a, determined in a separate Eu leaching experiment) from the used 5,000 μg l^{-1} PS-Eu particles exposure concentration in solution. We also performed a plant uptake experiment in which two plant seedlings were exposed to $Eu(TTA)_3$ alone at Eu concentrations approximately equal to 0.3% leakage from the PS-Eu particles exposure concentration in solution that was used. These were used as controls to estimate the potential leakage of Eu or Eu chelate from PS-Eu particles on the accumulation of Eu in the plants.

To evaluate plastic particle uptake from real soil, further experiments were performed by culturing the two plant species in sandy soil irrigated with treated wastewater. Treated wastewater was provided by a local municipal wastewater treatment facility and had the following characteristics: biological oxygen demand, 11.0 mg l^{-1}; chemical oxygen demand, 38 mg l^{-1}; total organic carbon, 49.9 mg l^{-1}; total nitrogen, 10.4 mg l^{-1}; total phosphorus, 11.3 μg l^{-1}; pH, 6.6; and electrical conductivity, 3.0 ms cm^{-1}. The treated wastewater was filtered through a 0.45 μm membrane and then used to perform plant uptake experiments in sandy soil culture conditions. Soil samples were collected in summer 2017, before sowing, from the top layer (0–20 cm) of a fluvo-aquic soil. The soil had a sandy loam texture (12% clay, 23% silt and 65% sand), a pH of 8.8, a total N content of 0.25 g kg^{-1} and a total organic C content of 3.3 g kg^{-1}. The cropping rotation system at the site where the soil was collected was wheat (*T. aestivum* L.) in winter and maize (*Zea mays* L.) in summer. The soil was first blended with river sand (50% v/v) to yield a soil–sand mixture. Triplicate soil–sand mixtures (250 g) were treated with a suspension of PS-Eu particles to reach a target concentration of 1 mg PS-Eu particles per kilogram soil or 10 mg PS-Eu particles per kilogram soil and placed in pots, followed by the addition of deionized water to 60% of the water holding capacity of the soil. Each pot was covered and sealed with plastic film containing small holes to maintain a relatively constant moisture content, and deionized water was added every four days if necessary. Wheat and lettuce seedlings were planted in the sandy soil and incubated in a growth chamber (as described above). The soils were irrigated daily with treated wastewater. Samples were collected after 14 days and immediately washed with deionized water prior to analysis.

Biological effects after exposure. A separate plant culture experiment was performed to investigate the potential effects of PS particle exposure on physiological and biochemical indicators in the two plants. Plants were randomly selected to be exposed to particles at 0, 100 or 5,000 μg particles per litre, of either the Eu-chelate-labelled PS-Eu particles or unlabelled PS particles. A nutrient solution without particles was used as a control. Three independent replicates were used for each treatment.

After harvesting at six days, the seedlings were gently removed from the beaker, and the roots were rinsed with deionized water thoroughly. The fresh weights of the seedlings were measured immediately. Net photosynthesis rate (μmol CO_2 m^{-2} s^{-1}), stomatal conductance (μmol H_2O m^{-2} s^{-1}) and transpiration rate (mmol H_2O m^{-2} s^{-1}) were determined using a portable photosynthetic system (LI-6400XTR, Li-Cor) at a photon flux density of 1,000 μmol m^{-2} s^{-1} and ambient CO_2 concentration of 400 μmol mol^{-1}.

For oxidative stress assays, root samples harvested at six days were homogenized in water (0.1 g tissue per 1 ml water). The samples were centrifuged at 3,000 r.p.m. for 5 min to remove the residues. The catalase activity was measured using kits from the Nanjing Jiancheng Bioengineering Institute, Nanjing, China.

It was analysed following the manufacturer's instructions with an UV–visible spectrophotometer (UV-1800, Mapada).

To study the stability of PS-Eu particles in the hydroponic exposure medium, the hydrodynamic diameter of the PS particles was measured at zero and six days using a zetasizer nanoZS90 (Malvern) for the 5,000 μg l^{-1} dose. SEM was used to study the possible morphological changes of PS particles in 20% Hoagland solution after exposure to plants. A scanning electron microscope (S-4800, Hitachi) was employed with an accelerating potential of 20 kV in high vacuum mode with backscatter detection. Images were captured at different magnifications. For each species, at least three plants per treatment group were examined. Digital images were captured using an EVO 40 scanning electron microscope (Zeiss). We also analysed the potential loss of Eu in the plants' exposure solution using a centrifugal ultrafiltration technique at the end of an exposure duration of six days, as described above. The concentration of total organic carbon was measured with a TOC-VCPH analyser (Shimadzu).

The mass balance of Eu in the exposure system was calculated by weighing the total amount of PS-Eu particles added to the system against the Eu concentrations in the different analysed compartments, that is, the solution samples, adsorption to beaker, adsorption to roots, and absorption on the roots and translocation to shoot tissues.

Fluorescence imaging of PS-Eu particles in plants. Following exposure to the PS-Eu particles, the roots of the wheat and lettuce plants were removed and washed thoroughly with distilled water. The digital images of the seedlings of lettuce and wheat were collected under 365 nm UV light. Subsequently, fresh root (mature zone) and stem (2 cm from the base of the stem) segments were collected and embedded in 4% agarose. The root and stem samples and the leaf blades (with the primary vein) were then sectioned into 40- and 100-μm-thick sections, respectively, using a vibrating microtome (VT1200S Vibrotome, Leica). Semithin sample sections were placed on a glass slide and covered with a coverslip. A few drops of phosphate buffer solution were added to maintain sample hydration. Then, the sections were characterized by luminescence imaging under a laboratory-use microscope. An inverted fluorescence microscope (TE 2000-E, Nikon) equipped with a 100 W Hg lamp, UV-2A filters (excitation filter, 330–380 nm; dichroic mirror, 400 nm; emission filter, >420 nm) and V-2A filters (excitation filter, 380–420 nm; dichroic mirror, 430 nm; emission filter, >450 nm), and a cooled colour CCD (charge-coupled device) camera system (RET-2000R-F-CLR-12-C, Qimaging) was used for the steady-state luminescence imaging measurements with an exposure time of 0.3 s. The microscope, equipped with a 30 W xenon flashlamp (Pulse300, Photonic Research Systems), a 100 W mercury lamp (C-LHG1, Nikon), a ×40 objective lens (CFI Plan Fluor ELWD DM 40 C, Nikon), epifluorescence filters (UV-2A, B-2A, G-2A; Nikon), a time-gated digital CCD camera system (Photonic Research Systems) and a cooled CCD camera (RET-2000R-F-CLR-12-C, Qimaging) was used for the time-gated luminescence imaging measurements with a delay time of 100 ms, a gate time of 1 ms, a lamp pulse width of 6 ms and an exposure time of 2 s. The time-gated luminescence images were rendered in pseudocolour with SimplePCI software.

Quantification of PS-Eu particles uptake into plants. Harvested plant root and shoot tissues from the two plant species grown in hydroponic and soil cultures were dried completely at 100 °C for 24 h before determining their dry weight. The root samples were washed with particular care to remove adsorbed particles before quantification. After digestion with a mixture of HNO_3 and H_2SO_4 (8:1, v/v, 4.5 ml) at 180 °C for 6 h, the samples were diluted with ultrapure deionized H_2O and filtered with 0.2 μm syringe filters (28145, VWR International). Eu was then analysed with ICP-MS (Agilent 7500i, Agilent Technologies). Standard reference material (spinach leaves (GBW10015)) obtained from the National Research Center for Certified Reference Materials of China with known iron and rare-earth-element concentrations was analysed with each batch of samples. The plant extraction method was verified by analysing the Eu recovery from the spinach leaf standard supplemented with two different concentrations of PS-Eu particles. Recovery of Eu from the plant tissues of the spiked samples was 103 ± 5%. The concentration of Eu was converted to the concentration of PS-Eu particles using the linear equation (Supplementary Fig. 2) obtained using exogenous PS-Eu particles after subtracting the background value from the control group. The root-to-shoot translocation factor was defined as the ratio of the calculated PS-Eu particles concentration in the shoots to the corresponding concentration in the roots. The bioconcentration factor was defined as the ratio of the calculated PS-Eu particles concentration in the roots to the corresponding concentration in the soils.

SEM. Samples from the roots, stems and fully expanded leaves near the primary veins of the plants grown in the hydroponic cultures were excised, sectioned into small pieces and frozen in liquid nitrogen. The samples were then freeze-dried and coated with gold for 60 s (~1 nm gold thickness) with a sputter coater (Cressington model 108, Ted Pella). The samples were then examined with a Hitachi S-4800 field emission scanning electron microscope equipped with an EX-350 energy-dispersive X-ray microanalyser (HORIBA EMAX Energy, Hitachi). The samples were dried at 40 °C and plated with Pt using a Hitachi E-1045 ion sputter coater before analysis. The SEM instrument was operated at an electron accelerating voltage of 3.0 kV, and secondary electron images were obtained at high resolution. Images were captured at various magnifications. For both plant species, at least three individual plants from each treatment group were examined.

Statistical analysis. Data were evaluated by one-way analysis of variance followed by the Duncan's multiple range test when appropriate. Statistical analysis was performed using the software package IBM SPSS Statistics (v.16.0). A difference was considered significant when $P < 0.05$. Values are expressed as mean ± s.d.

Data availability

Source data are provided with this paper. Additional datasets related to this study are available from the corresponding author upon reasonable request.

References

41. Melby, L. R., Abramson, E., Caris, J. C. & Rose, N. J. Synthesis fluorescence of some trivalent lanthanide complexes. *J. Am. Chem. Soc.* **86**, 5117–5125 (1964).
42. Lu, S. L., Qu, R. J. & Forcada, J. Preparation of magnetic polymeric composite nanoparticles by seeded emulsion polymerization. *Mater. Lett.* **63**, 770–772 (2009).
43. Hoagland, D. R. & Arnon, D. I. *The Water-Culture Method for Growing Plants without Soil.* Circular No. 347 (Univ. of California, College of Agriculture, 1938).
44. Grimme, S., Ehrlich, S. & Goerigk, L. Effect of the damping function in dispersion corrected density functional theory. *J. Comp. Chem.* **32**, 1456–1465 (2011).
45. Dunning Jr, T. H. & Hay, P. J. in *Modern Theoretical Chemistry* Vol. 3 (ed. Schaefer III, H. F.) 1–28 (Plenum, 1977).
46. Frisch, M. J. et al. *Gaussian 16* v.C.01 (Gaussian, 2016).

Acknowledgements

Y.L. gratefully acknowledges the Major Program of the National Natural Science Foundation of China (grant no. 41991330), the financial support by the Key Research Program of Frontier Sciences, Chinese Academy of Sciences (grant no. QYZDJ-SSW-DQC015) and the National Nature Science Foundation of China (grant no. 41877142). L.L. acknowledges the National Nature Science Foundation of China (grant no. 42177040). W.J.G.M.P. benefited from the European Union's Horizon 2020 research and innovation programme (PLASTICFATE, grant agreement no. 965367). We thank B. Song and J. Yuan at Dalian University of Technology for their kind help with the time-gated luminescence technique. We express our gratitude to C. Liu for his kind help in the calculation of the relative stability constants for metal complexes.

Author contributions

Y.L. managed the whole project, designed all the experiments and jointly wrote the manuscript. L.L. conducted the uptake experiments and wrote the manuscript. Y.F. measured the metal content in the particles and plants as well as the release of the Eu in the solutions. R.L. inspected the plant tissue using a confocal laser scanning microscope and time-gated luminescence imaging technique. J.Y. examined the samples with a scanning electron microscope and collected the images. R.L. and C.T. analysed the biological effect and analysed the enzyme activity. W.J.G.M.P. helped with manuscript revision and data analysis. All authors contributed to the results, discussion and manuscript writing.

Competing interests

The authors declare no competing interests.

Additional information

Supplementary information The online version contains supplementary material available at https://doi.org/10.1038/s41565-021-01063-3.

Correspondence and requests for materials should be addressed to Yongming Luo.

Nature Nanotechnology thanks Ilaria Corsi, Livius Muff and Fabienne Schwab for their contribution to the peer review of this work.

Reprints and permissions information is available at www.nature.com/reprints.